

Coherence Properties of Guided-Atom Interferometers

H. Kreutzmann,^{1,*} U.V. Poulsen,¹ M. Lewenstein,¹ R. Dumke,² W. Ertmer,² G. Birkl,² and A. Sanpera¹

¹*Institut für Theoretische Physik, Universität Hannover, 30167 Hannover, Germany*

²*Institut für Quantenoptik, Universität Hannover, 30167 Hannover, Germany*

(Received 10 September 2003; published 21 April 2004)

We present a detailed theoretical investigation of the coherence properties of beam splitters and Mach-Zehnder interferometers for guided neutral atoms. We show that such a setup permits coherent wave packet splitting and leads to the appearance of interference fringes for both single-mode and thermal input states, evidencing thus the robustness of the interferometer.

DOI: 10.1103/PhysRevLett.92.163201

PACS numbers: 39.20.+q, 32.80.Pj

The investigation and exploitation of the wave properties of atomic matter is of great interest for fundamental as well as applied research and constitutes, therefore, one of the most active research areas in atomic physics and quantum optics. Of special interest is the field of atom interferometry [1]. For an interferometer, it is crucial that the beam splitters and mirrors are coherent, i.e., they must not disturb the phase of the matter wave in an uncontrollable fashion. Then a phase shift in one of the paths results in a change of the output signal, and any external influence inducing a phase shift is, in principle, accessible to measurement. Compared to light interferometry, matter wave interferometry with cold atoms offers a much higher sensitivity for certain applications [1]. Furthermore, atoms couple efficiently to a wider variety of external interactions, thus extending the applicability of interferometric measurements [1].

With the use of guided atoms [2–4], miniaturized setups for matter wave interferometry with increased stability, large beam separation, and large enclosed areas become possible [4–7]. These features are specifically appealing to measurements of inertial forces [8] and to the investigation of Bose-Einstein condensates in microstructures [9]. In order to assess the level of performance that can be reached with realistic setups, coherence and interference (also for mixed input states) as well as non-perfect beam splitters have to be investigated in detail.

In this Letter we study guided-atom interferometers by solving numerically the time dependent Schrödinger equation for realistic, experimentally accessible configurations. Our study addresses the main issues of atom propagation in guides, as well as coherence and interference using X-shaped guided-atom beam splitters [2–4,10]. Our calculations are closely related to the scheme in which neutral atoms are guided in dipole potentials. These potentials are created by microfabricated cylindrical lenses which focus laser light into arrays of line foci [4,11]. For light detuned below an atomic resonance (i.e., red detuned) each line focus creates a guiding structure for atoms with Gaussian confining potentials in the two transverse directions and a flat potential in the longitudinal direction. Beam splitters are achieved by crossing

two line foci at some angle [3,4]. The splitting of the atomic wave packet is done in coordinate space without affecting the internal state. Nevertheless, internal state selective interferometry is also possible. Many of the experimental prerequisites of this scheme such as atom guides, beam splitters, and even geometries composing a complete Mach-Zehnder interferometer for atoms have been realized already [4].

During the splitting process the system might exhibit quantum reflections and tunneling between adjacent guides. We demonstrate, however, that such a beam splitter is coherent even for a thermal distribution of atoms with an average energy far exceeding the level spacing of the transverse confinement.

To study the properties of the beam splitter and the interferometer we use the split-operator method to solve numerically the time dependent Schrödinger equation

$$i\hbar \frac{\partial \Psi(x, y, t)}{\partial t} = \left[-\frac{\hbar^2}{2m} \nabla^2 + V(x, y) \right] \Psi(x, y, t), \quad (1)$$

where the potential $V(x, y)$ includes the guiding potentials and any other potential considered in the calculation. For simplicity, we shall assume throughout this paper that the atomic wave packet is tightly confined in the third dimension so that the dynamics is well described within a two-dimensional treatment.

The central element of any interferometer is the beam splitter. Consequently, we start our discussion with a detailed analysis of an X-shaped guided-atom beam splitter (BS) created by crossing two identical waveguides L_i and L_j at an angle γ :

$$U_{\text{BS}}(x, y) = U_i(x, y) + U_j(x \cos \gamma - y \sin \gamma, y \cos \gamma + x \sin \gamma).$$

Each waveguide consists of a Gaussian potential of depth U_0 and width σ centered around some x_0 : $U_i(y, x) = -U_0 \exp[-(x - x_0)^2/2\sigma^2]$. Coupling from one guide to the other occurs for any angle $\gamma \neq 90^\circ$. We observe, however, that the doubling of the potential depth at the crossing of the two waveguides induces quantum reflections and a highly nonadiabatic dynamics for typical initial momenta of the atomic wave packet. These effects

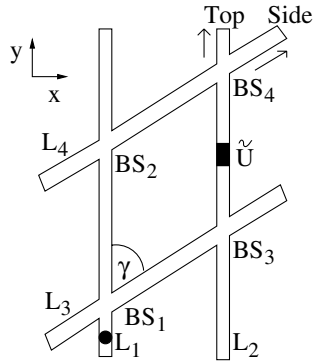


FIG. 1. Schematic view of a Mach-Zehnder interferometer for guided atoms using four identical waveguides crossing at an angle γ . The initial atomic wave packet is represented by a dot in waveguide L_1 below the first beam splitter (BS_1). The location of the phase shift potential $\tilde{U}(x, y)$ is also depicted.

are clearly undesirable for interferometry. For a micro-optical realization of the waveguides, they can be easily avoided by reducing the light intensity at the crossing through overlay of an absorptive mask or by adding a compensating extra potential (e.g., a blue detuned laser field) so that the depth of the total potential at the crossing is equal to the one of each waveguide alone. In our simulations we have taken into account that this compensation might not be perfect.

Our choice of parameters closely matches the relevant experimental parameters of Refs. [4,11] where ^{85}Rb atoms are guided in dipole potentials, far detuned below the $5S_{1/2} \rightarrow 5P_{3/2}$ transition (780 nm). An appropriate experimental configuration could consist of waveguides of width $\sigma = 0.54 \mu\text{m}$ (corresponding to a Gaussian beam with $1/e^2$ waist $w_0 = 1.1 \mu\text{m}$) at a laser wavelength of 830 nm and an intensity of $I = 1.1 \times 10^5 \text{ W/cm}^2$ (less than 1 W of required laser power). Then the potential depth is $U_0 = 75 \mu\text{K}$, the ground state vibrational frequency $\omega = 160 \times 10^3 \text{ s}^{-1}$, and the spontaneous scattering rate $\Gamma_S = 2.6 \text{ s}^{-1}$ (thus it can be neglected in our discussion).

In our simulations we assume as input an atomic wave packet located in one of the waveguides (L_1 in Fig. 1) at a typical distance of $2.5 \mu\text{m}$ from BS_1 . The initial atomic wave packet has a Gaussian profile along the longitudinal direction of the waveguide with a mean momentum p_y and a spread of Δp_y . Values of the mean momentum are in the range of 5–10 recoil momenta p_r ($p_r = \sqrt{2\hbar m \omega_r}$, $\omega_r = 24 \times 10^3 \text{ s}^{-1}$), with a momentum spread $\Delta p_y = 2p_r$. In general, the initial transverse state of the atomic wave packet can be described by a thermal mixture

$$\rho = \frac{1}{Z} \sum_{n=0}^{\infty} e^{-E_n/k_B T} |\varphi_n\rangle\langle\varphi_n|, \quad (2)$$

where $|\varphi_n\rangle$ denotes the n th eigenstate of the guiding potential $U(x)$, E_n denotes its energy, and Z ensures proper normalization. Assuming an atomic sample at a

temperature of $T = 20 \mu\text{K}$ our set of parameters leads to a mean quantum number of $\langle n \rangle \approx 16$.

The splitting of the initial wave packet depends on its initial transverse state, its initial longitudinal momentum $p_y = mv_y$, and on the angle γ between the guides. In order to achieve efficient deflection in the beam splitter, the atomic wave packet has to spend enough time at the intersection. Defining the crossing time as $t_c = \sigma/v_y$ efficient splitting requires $t_c \gtrsim \hbar/E_n$. For a fixed angle γ and a fixed initial momentum p_y , we observe that the dependence of the splitting ratio on the initial transverse state $|\varphi_n\rangle$ is very strong. This is displayed in Fig. 2, where we plot the fraction of atoms transmitted towards BS_2 (T) and the fraction deflected towards BS_3 (D) as a function of the initial transverse state for $\gamma = 45^\circ$ and two different initial longitudinal momenta, $p_y = 10p_r$ and $p_y = 5p_r$. To “count” the number of deflected (transmitted) atoms we use an absorbing box in L_3 (L_1) after the beam splitter and integrate the loss of norm in each box with time. The transmitted and deflected fraction do not always add up to unity. The missing fraction consists of atoms backscattered into the downward sections of waveguides L_1 and L_3 . For $p_y = 10p_r$, an approximately 50/50 splitting ratio occurs for transverse initial states with quantum numbers $n \approx 8$ –11. Losses due to backscattering are very small in this case. For $p_y = 5p_r$ the optimal splitting ratio occurs for $n \approx 2$ –3 although losses are now significantly higher (i.e., 40% transmitted, 30% deflected, and 30% losses for $n = 3$). In both cases, the deflected fraction is narrowly peaked around its maximum evidencing that even for thermal input states, efficient splitting occurs only for a narrow group of states around the optimal one. Notice also that the waveguide ground state ($\rho_0 = |\varphi_0\rangle\langle\varphi_0|$) splits extremely inefficiently. The following simple picture helps to understand the selection of the optimal state $|\varphi_n\rangle$ for a given initial momentum p_y and angle γ : At the intersection, the wave packet is no longer confined transversely and,

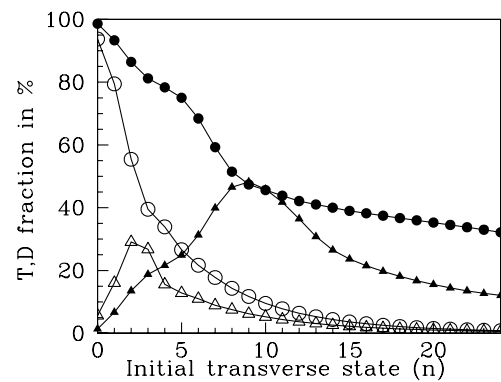


FIG. 2. Splitting efficiency of guided-atom beam splitter: transmitted (T) (circles) and deflected (D) (triangles) fraction of the incoming wave packet as function of the initial transverse state φ_n of the waveguide for $\gamma = 45^\circ$. Solid symbols correspond to $p_y = 10p_r$ and open symbols to $p_y = 5p_r$.

therefore, expands according to its initial transverse momentum distribution. Optimal splitting occurs for typical transverse momenta $p_x = \sqrt{2mE_n}$ fulfilling $p_x \approx p_y \tan \gamma$. Approximating the center of the waveguide by a harmonic potential of frequency ω one obtains the estimate $n_{\text{opt}} \approx p_y^2 \tan^2(\gamma)/(2m\hbar\omega)$. Lower transverse states can be made optimal by lowering p_y and/or lowering γ . A lower n_{opt} also implies fewer states within the peak of non-negligible splitting ratios thus enhancing the filtering effect of the beam splitter. Despite the simplicity of the argument, it agrees well with our results depicted in Fig. 2 and with our simulations for different initial longitudinal momenta p_y and angles γ . Only for angles $\gamma \leq 25^\circ$ we find strong deviations from our estimate since there back-scattering and tunneling start to play an important role in the splitting dynamics.

The coupling between transverse and longitudinal degrees of freedom in the splitting process results in a complex dynamics after the beam splitter. We calculate the longitudinal phase profile of each wave packet before it reaches the next beam splitter. The transmitted wave packet propagates along the waveguide L_1 almost without distortion and its phase profile agrees well with the phase profile of a wave packet propagating freely in a transverse harmonic potential [12]. The motion along L_3 is more involved. Although the overall behavior of the phase resembles the one of the wave packet along L_1 , even for a single-mode input initial state, the wave packet propagating along L_3 exhibits transverse oscillatory motion of frequency ω . This is caused by the excitation of a coherent superposition of transverse states and clearly demonstrates that the splitting process is nonadiabatic. Such motion has to be taken into account to optimize the efficiency of the full Mach-Zehnder interferometer.

The full interferometer is realized by appropriately crossing four identical waveguides. Because of numerical limitations, we constrain the distance between L_1 and L_2 to about $7 \mu\text{m}$ [13]. Atoms loaded in the waveguide L_1 with initial momentum p_y propagate to the first beam splitter BS_1 and are then guided through L_1 and L_3 towards BS_2 and BS_3 , respectively. Here BS_2 and BS_3 act as mirrors, but due to the additional output ports also establish new loss channels. Note that this Mach-Zehnder configuration is not symmetric even for 50/50 beam splitters, since, as we have already discussed, the dynamics in the different arms of the interferometer becomes distinct after the first beam splitter. Hence following splitting processes in the two arms are no longer equivalent. This lack of symmetry excludes the possibility of achieving 100% visibility (defined as the amplitude [i.e., $1/2$ (max-min)] of the modulation in the top output divided by the average in the top output) and demands optimization strategies to improve the visibility.

To demonstrate that coherence is preserved during the propagation through the full interferometer, we calculate the output signals after the final beam splitter BS_4 as a function of the depth d of an additional potential

$\tilde{U}(x, y) = -d U_0 e^{-(x-\bar{x}_0)^2/2\sigma^2} e^{-(y-\bar{y}_0)^2/2\sigma^2}$ which is inserted in one of the arms of the interferometer (between BS_3 and BS_4) to induce a phase shift between both arms. This extra potential, which can be either attractive or repulsive depending on the sign of d , has a Gaussian profile along the waveguide and smoothly lowers ($d > 0$) or increases ($d < 0$) the potential depth of that part of the waveguide. Our results are summarized in Figs. 3 and 4. Clear periodic modulations (interference fringes) in the number of atoms exiting each output port (labeled top and side outputs for clarity) appear as a function of d for both single-mode (Fig. 3) and thermal initial state (Fig. 4).

For the single-mode case, we choose, for simplicity, the ground state with mean longitudinal momentum $p_y = 10p_r$ and momentum spread $\Delta p_y = 2p_r$ as initial state. In Fig. 3(a), we display the fraction of atoms at the top output versus d . The expected modulation of the atom number as a function of d is clearly visible. We compare the period of the oscillation with the one obtained using a simplified model of the phase shift ϕ introduced by the additional potential \tilde{U} using the classical action $S = \int dt \mathcal{L}$, where \mathcal{L} is the Lagrangian. Despite the oversimplification of this model, the calculated period is only a few % too small for low values of d . For larger d the increase in the oscillation period is more accurately described using a WKB approximation.

For the ground state case, the total atom number exiting both outputs of the interferometer is only $\approx 1\%$ of the initial atom number (typically 10^4 atoms in experiments) and the visibility is low ($\approx 2\%$) since the ground state splits very inefficiently. Better visibilities can be achieved by choosing as input the state with the optimal splitting ratio (c.f. Fig. 4) and using an optimized geometry. An optimized geometry aims at equalizing as much as possible the contributions from both arms of the interferometer to the final signal. This can be accomplished by choosing the distance between the waveguides L_1 and L_2 such that the wave packet that propagates in L_3 with transverse oscillations enters the beam splitter BS_3 with a mean transverse momentum appropriate to maximize the fraction of atoms deflected towards BS_4 . This

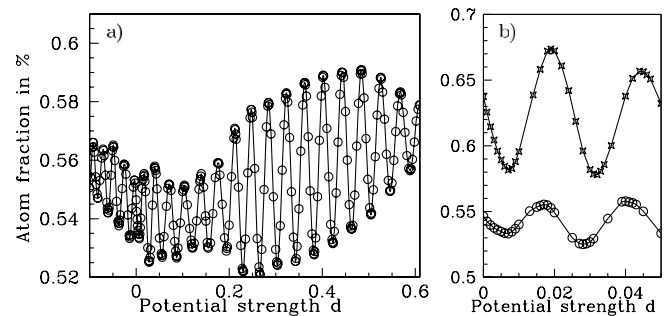


FIG. 3. (a) Atom fraction (in % of the input atom number) in the top output versus the strength d of $\tilde{U}(x, y)$ for $\rho = |\varphi_0\rangle\langle\varphi_0|$. (b) Same as (a) (circles) and the signal for an optimized geometry (stars).

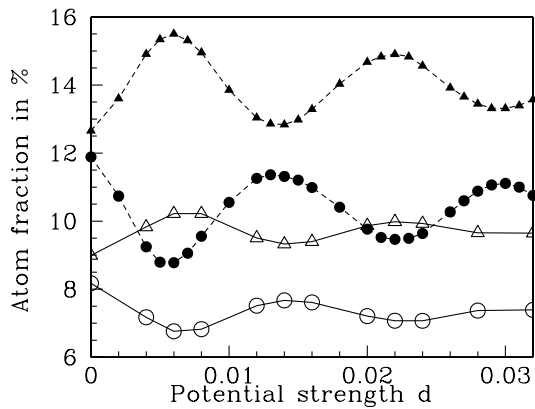


FIG. 4. Atom fraction (in %) in the side (triangles) and top (circles) outputs versus the strength d of $\tilde{U}(x, y)$. Solid symbols correspond to the (optimal) input state $n = 2$, open symbols to an initial thermal state at $T = 20 \mu\text{K}$.

optimization immediately leads to a visibility of $\approx 7\%$ as shown in Fig. 3(b).

Experimentally, a more realistic scenario corresponds to an initial wave packet with a thermal occupation of transverse states [Eq. (2)]. For this case, we calculate the final output signal as a classical (Boltzmann) weighted average of the signal obtained for each transverse state $|\varphi_n\rangle$ separately. In our calculations, we now use an optimized geometry but also consider, that the compensation of the double potential in the beam splitters is not perfect by allowing a 5% mismatch in potential depth at the beam splitters. Figure 4 displays the interference fringes for an initial state corresponding to all atoms in the optimal splitting state $\rho = |\varphi_2\rangle\langle\varphi_2|$ (c.f. Fig. 2) and for a thermal (multimode) state corresponding to $T = 20 \mu\text{K}$. In both cases $p_y = 5p_r$, $\Delta p_y = 2p_r$, and $\gamma = 45^\circ$. Since the beam splitter is state selective, interference fringes are mostly due to states with a good splitting ratio as evidenced by the fact that maxima and minima appear approximately at the same positions in both cases. The combined atom number for the optimal state is about 24% of the initial atom number, with visibilities up to 15%. (Visibilities up to $\approx 23\%$ can be obtained for $\rho = |\varphi_1\rangle\langle\varphi_1|$ but with a lower total signal). For the thermal initial state the different splitting ratios corresponding to the different transverse states lower the total output signal to $\approx 17\%$ but with visibilities up to 10%. This clearly demonstrates the persistence of coherence and interference even for thermal input states and allows for the operation of the interferometer as a multimode device. In fact, compared to the zero temperature case (ground state), a thermal state which inherently contains the optimal state will dramatically improve the performance of the interferometer.

In summary, our simulations provide strong evidence of the feasibility of guided-atom interferometry. We have

shown that an X-shaped beam splitter created by appropriately crossing two identical waveguides (with the doubling of the potential properly compensated) preserves coherence and acts analogously to a “color filter,” selecting only a few optimal transverse states which contribute to the final signal. In this way coherence is robustly preserved throughout the interferometer and temperature is not necessarily a limitation for the observation of interference fringes. Obviously, experimental noise (such as statistics in the atom number) will reduce the observable fringe visibility, but with predicted visibilities as high as 15% the experimental observation of interference fringes will be feasible.

This work is supported by the *Deutsche Forschungsgemeinschaft* (SFB 407) and the *European Commission* (RTN Cold Quantum Gases, RTN ATOM CHIPS, and IST project ACQP).

*Electronic address: kreutzm@itp.uni-hannover.de

- [1] *Atom Interferometry*, edited by P. R. Berman (Academic Press, San Diego, 1997), and references therein.
- [2] R. Folman *et al.*, *Adv. At. Mol. Opt. Phys.* **48**, 263 (2002), and references therein.
- [3] O. Houde, D. Kadio, and L. Pruvost, *Phys. Rev. Lett.* **85**, 5543 (2000).
- [4] R. Dumke *et al.*, *Phys. Rev. Lett.* **89**, 220402 (2002).
- [5] E. A. Hinds, C. J. Vale, and M. G. Boshier, *Phys. Rev. Lett.* **86**, 1462 (2001).
- [6] W. Hänsel, J. Reichel, P. Hommelhoff, and T.W. Hänsch, *Phys. Rev. A* **64**, 063607 (2001).
- [7] E. Andersson *et al.*, *Phys. Rev. Lett.* **88**, 100401 (2002).
- [8] A. Peters, K. Y. Chung, and S. Chu, *Nature (London)* **400**, 849 (1999); J. M. McGuirk *et al.*, *Phys. Rev. A* **65**, 033608 (2002); T. L. Gustavson, P. Bouyer, and M. A. Kasevich, *Phys. Rev. Lett.* **78**, 2046 (1997); T. L. Gustavson, A. Landragin, and M. A. Kasevich, *Classical Quantum Gravity* **17**, 2385 (2000).
- [9] H. Ott *et al.*, *Phys. Rev. Lett.* **87**, 230401 (2001); A. E. Leanhardt *et al.*, *ibid.* **89**, 040401 (2002); M. P. A. Jones, C. J. Vale, D. Sahagun, B. V. Hall, and E. A. Hinds, *ibid.* **91**, 080401 (2003); W. Hänsel, P. Hommelhoff, T.W. Hänsch, and J. Reichel, *Nature (London)* **413**, 498 (2001); S. Schneider *et al.*, *Phys. Rev. A* **67**, 023612 (2003).
- [10] M. D. Girardeau, K. K. Das, and E. M. Wright, *Phys. Rev. A* **66**, 023604 (2002); J. A. Stickney and A. A. Zozulya, *Phys. Rev. A* **68**, 013611 (2003).
- [11] G. Birkl, F. B. J. Buchkremer, R. Dumke, and W. Ertmer, *Opt. Commun.* **191**, 67 (2001).
- [12] C. Bordé, *C.R. Acad. Sci. Ser. IV* **2**, 509 (2001).
- [13] Convergence and wave packet spreading effects were studied by performing some runs with a waveguide separation of $21 \mu\text{m}$. Our results show that spreading does not affect the visibility of the interference fringes.